Thermoelectric properties and efficiency measurements under large temperature differences

A. Muto,[1] D. Kraemer,[1] Q. Hao,[1] Z. F. Ren,[2] and G. Chen[1]
[1]*Department of Mechanical Engineering, Massachusetts Institute of Technology, Cambridge, Massachusetts 02139, USA*
[2]*Department of Physics, Boston College, Chestnut Hill, Massachusetts 02467, USA*

(Received 26 June 2009; accepted 4 August 2009; published online 1 September 2009)

The maximum efficiency of a thermoelectric generator is determined by the material's dimensionless figure of merit *ZT*. Real thermoelectric material properties are highly temperature dependent and are often measured individually using multiple measurement tools on different samples. As a result, reported *ZT* values have large uncertainties. In this work we present an experimental technique that eliminates some of these uncertainties. We measure the Seebeck coefficient, electrical conductivity, and thermal conductivity of a single element or leg, as well as the conversion efficiency, under a large temperature difference of 2–160 °C. The advantages of this technique include (1) the thermoelectric leg is mounted only once and all measurements are in the same direction and (2) the measured properties are corroborated by efficiency measurements. The directly measured power and efficiency are compared to the values calculated from the measured properties and agree within 0.4% and 2%, respectively. The realistic testing conditions of this technique make it ideal for material characterization prior to implementation in a real thermoelectric generator. © *2009 American Institute of Physics.* [doi:10.1063/1.3212668]

I. INTRODUCTION

Recent years have witnessed a trend of rising electricity costs and an emphasis on energy efficiency. Thermoelectric (TE) devices can be used either as heat pumps for localized environmental control or heat engines for harvesting waste heat, and such usages can potentially increase the overall efficiency in many systems. For TE power generators to be successful, research progress at the device level must be made to validate materials and to guide system design.[1]

The performance of a TE material is characterized most commonly by its so-called dimensionless figure of merit $Z\bar{T}=\alpha^2\bar{T}/\rho k$ or "intrinsic *ZT*." The three temperature-dependent properties or "intrinsic properties" $\alpha(T)$, $\rho(T)$, and $k(T)$ are the Seebeck coefficient, electrical resistivity, and thermal conductivity, respectively, and $\bar{T}$ is the mean absolute temperature. The intrinsic properties are highly temperature dependent, and to measure each represents a formidable task.

Typically one of two methods is used to characterize a TE material over a small temperature difference: (1) the Harman method[2] and (2) the three intrinsic properties are measured independently over small temperature differences.[3] The original Harman method is used to measure $\rho(T)$ and $Z\bar{T}(T)$ over small temperature differences.[2,4] This technique has many variations and has been applied to bulk modules and thin films alike.[5,6] The drawbacks are that it only works over small temperature differences and requires adiabatic boundary conditions that can be difficult to satisfy.[7] The second method uses different measurement systems for each individual property.[3,8,9] Often, all three properties are not measured on the same sample or along the same direction. The second method is very time consuming, and both methods can result in large uncertainties in $Z\bar{T}(T)$, often greater than 10%.[10]

TE power generators usually operate under large temperature differences up to hundreds of degrees centigrade. If $Z\bar{T}$ is temperature independent, the maximum efficiency $\eta_{\max}$ of a TE element can be expressed as[3,11]

$$\eta_{\max}=\frac{T_H-T_C}{T_H}\frac{\sqrt{1+Z\bar{T}}-1}{\sqrt{1+Z\bar{T}}+T_C/T_H}, \tag{1}$$

where T_H is the hot side temperature and T_C is the cold side temperature. However, since the intrinsic properties vary strongly with temperature along the length of the element or "leg," Eq. (1) is not applicable and often numerical solutions must be used to obtain the actual device efficiency.[12] Furthermore, in real TE applications additional effects must also be considered such as electrical contact resistance at the junctions of the TE legs and radiation losses from the leg side walls.[13,14]

In this work we develop methods to characterize a single TE leg operating under a large temperature difference. We aim to extract the three intrinsic properties of a single leg and verify the results by comparing the predicted power conversion efficiency from the property measurements to the actual measured efficiency. Such testing conditions provide a more realistic examination of actual TE device performance and should thus support the development and design of future TE power generators.

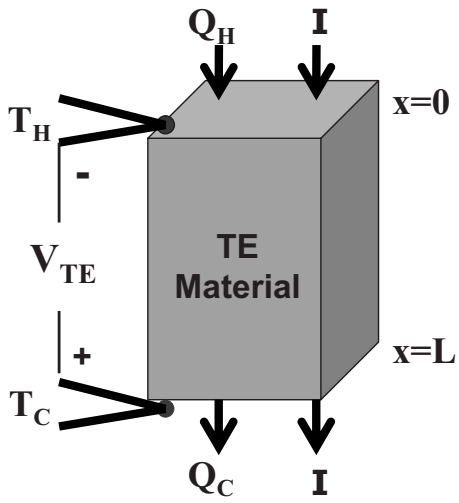

FIG. 1. Illustration of a *p*-type TE leg under working conditions.

II. MATHEMATICAL FORMULATION

A. Governing equation

Figure 1 is a general schematic of a *p*-type TE sample under test, where the hot side heat transfer rate Q_H enters from the top at T_H and the cold side heat transfer rate Q_C exits the bottom at T_C. The temperature is measured by thermocouples, and ΔT ranges from 2 °C to 160 °C. The electrical current I enters from the top and exits through the bottom of the sample, and V_{TE} is the TE voltage measured across the leg at the position of the thermocouples. We will directly measure the energy balance over the sample, which includes Q_H, Q_C, and the electric power $P_e=IV_{\mathrm{TE}}$. It will be shown that since the temperature difference across the leg is large it is useful to characterize the TE leg in terms of its effective properties, resulting in an "effective ZT," $Z\bar{T}_{\mathrm{eff}}(T_H,T_C)$. We define three classes of interrelated properties.

- "Device properties" are the directly measurable values, including the heat transfer rates, Seebeck voltage, and electrical resistance.
- "Effective properties" $\alpha_{\mathrm{eff}}(T_H,T_C)$, $k_{\mathrm{eff}}(T_H,T_C)$, and $\rho_{\mathrm{eff}}(T_H,T_C)$ are obtained directly from device properties measurement when the hot side is at T_H and cold side at T_C, or can be calculated by integrating the intrinsic properties over the temperature interval.
- "Intrinsic properties" $\alpha(T)$, $\rho(T)$, and $k(T)$ are properties of the materials at each temperature as previously defined, which will be extracted from the effective properties.

The constitutive relations for one-dimensional heat flux q and current density J are as follows:[15]

$$q = JT\alpha - k\frac{dT}{dx}, \tag{2}$$

$$J = -\frac{1}{\rho}\frac{dV_{\mathrm{TE}}}{dx} - \frac{\alpha}{\rho}\frac{dT}{dx}. \tag{3}$$

An energy balance over a one-dimensional differential element of a TE leg yields

$$A\frac{d}{dx}\left(k\frac{dT}{dx}\right) - IT\frac{d\alpha}{dx} + I^2\frac{\rho}{A} - \varepsilon\sigma_{\mathrm{sb}}P(T^4 - T_\infty^4) = 0, \tag{4}$$

with four terms on the left hand side representing the heat conduction, the Thompson heat, the Joule heat, and the radiation loss. Here A is the cross sectional area, ε is the emissivity, σ_{sb} is the Stephan–Boltzmann constant, P is the perimeter, and T_∞ is the ambient temperature. The leg is kept under high vacuum (5×10^{-5} Torr) such that natural convection and air conduction can be neglected.

B. Device properties measurement under large ΔT

The measured device properties are the open circuit Seebeck voltage V_S, the open circuit heat transfer rates $Q_{H,OC}$, $Q_{C,OC}$, and the electrical resistance of the leg R. Measuring these device properties directly as a function of temperature enables us to determine the effective properties, and finally solve for the intrinsic properties. In general V_{TE} is composed of a Seebeck voltage and an Ohmic voltage drop. During the properties measurement $I=0$, it follows from Eq. (3) that $V_{\mathrm{TE}}=V_S$ and is related to $\alpha_{\mathrm{eff}}(T_H,T_C)$ and $\alpha(T)$ by

$$V_S(T_H,T_C) = \alpha_{\mathrm{eff}}(T_H,T_C)\Delta T = \int_{T_C}^{T_H}\alpha(T)dT. \tag{5}$$

Equation (4) is reduced to only the heat conduction and the radiation terms and can be solved to give expressions for $k_{\mathrm{eff}}(T_H,T_C)$ and $k(T)$

$$Q_{H,OC}(T_H,T_C) = \frac{A}{L}k_{\mathrm{eff}}(T_H,T_C)\Delta T = \frac{A}{L}\int_{T_C}^{T_H}kdT + Q_{\mathrm{rad}}, \tag{6}$$

$$Q_{C,OC}(T_H,T_C) = Q_{H,OC} - Q_{\mathrm{rad,side}} = \frac{A}{L}\int_{T_C}^{T_H}kdT + Q_{\mathrm{rad}} - Q_{\mathrm{rad,side}}. \tag{7}$$

Here, Q_{rad} is the additional heat transfer rate on the hot side due to radiation from the side walls and $Q_{\mathrm{rad,side}}$ is the total radiation loss from the side walls (see Appendix). The geometry of the leg was chosen to minimize the effects of radiation, where $Q_{\mathrm{rad,side}}<2\%$ of $Q_{H,OC}$ and $Q_{\mathrm{rad}}<Q_{\mathrm{rad,side}}$. The heat transfer rates $Q_{H,OC}$ and $Q_{C,OC}$ are measured by a calibrated heater on the hot side and a heat flux sensor on the cold side, which will be described in more detail in Sec. III.

The electrical resistance is measured by a four-wire ac method where V_{TE} is the sense voltage.[3] The resistance measurement is applied in the limit that the current is small such that the Joule heat term can be neglected and the modulation frequency is high such that the Peltier heat alternates sign and cancels due to periodic heating and cooling at the junction. The electrical resistance R, is related to $\rho_{\mathrm{eff}}(T_H,T_C)$ and $\rho(T)$ by

$$R(T_H,T_C)=\frac{L}{A}\rho_{\text{eff}}(T_H,T_C)=\frac{1}{A}\int_{T_H}^{T_C}\frac{\rho dT}{\frac{dT}{dx}}\approx\frac{L}{A}\frac{\int_{T_C}^{T_H}k\rho dT}{\int_{T_C}^{T_H}kdT}, \tag{8}$$

whereby we have neglected the radiation term to approximate the temperature gradient as $dT/dx\approx -Q/kA$, where $Q=(A/L)\int_{T_C}^{T_H}kdT$ is the conducted heat, which is constant.

C. Efficiency

Unlike the device properties measurement which is conducted under the open circuit condition, the efficiency η must be measured when electrical current flows through the leg. The efficiency is defined as

$$\eta=\frac{P_e}{Q_H}=\frac{P_e}{Q_C+Q_{\text{rad,side}}+P_e}, \tag{9}$$

where the electrical power output P_e can be obtained from Eq. (3),

$$P_e=IV_S-I^2R=IV_{\text{TE}}. \tag{10}$$

Power is produced when the voltage has increased in the direction of current flow. In this way we use a current source to control I and measure V_{TE}, another method would be to measure the power dissipated over an adjustable resistor.[16,17] Both methods are equally valid, but experimentally the current source method has many advantages. We integrate Eq. (4) twice with respect to x and apply the boundary conditions illustrated in Fig. 1 to solve for the temperature gradient. The temperature gradient is then used to evaluate Q_H and Q_C from Eq. (2),

$$Q_C=IT_C\alpha(T_C)+Q_{C,OC}+\frac{1}{2}I^2R+\frac{1}{2}I\beta, \tag{11}$$

$$Q_H=IT_H\alpha(T_H)+Q_{H,OC}-\frac{1}{2}I^2R-\frac{1}{2}I\beta, \tag{12}$$

where the Thompson heat is written as

$$\beta(T_H,T_C)=\int_{T_C}^{T_H}T\frac{d\alpha}{dT}dT. \tag{13}$$

Equations (11) and (12) appear similar to the constant property heat transfer rate equations[3,11,18] but remember that in this case, R and β are the temperature integrated quantities described above and $Q_{H,OC}$, $Q_{C,OC}$ include the effects of sidewall radiation. The factors of $\frac{1}{2}$ in front of the Joule heat and Thompson heat terms are the result of an approximation that assumes both heating terms are distributed uniformly throughout the material such that half goes to the hot side and half goes to the cold side. If ρ, $Td\alpha/dT$ are independent of temperature then the factors of $\frac{1}{2}$ are exact (see Appendix). When solving for R during power generation we make a second approximation that the temperature gradient is defined by the intrinsic thermal conductivity alone as we have done in Eq. (8).

D. Effective *ZT*

If we approximate $\alpha(T_H)\approx\alpha(T_C)=\alpha_{\text{eff}}$, then the Thompson heat term drops out and Eq. (9) can be written in terms of the effective properties. In the same way $Z\bar{T}(T)$ was derived for intrinsic properties[3,11] we can define $Z\bar{T}_{\text{eff}}(T_H,T_C)$ based on the effective properties,

$$Z\bar{T}_{\text{eff}}=\frac{\alpha_{\text{eff}}^2\bar{T}}{\rho_{\text{eff}}k_{\text{eff}}}=\frac{V_S^2\bar{T}/|\Delta T|}{RQ_H}. \tag{14}$$

It can be used to solve for the maximum conversion efficiency [Eq. (1)] and maximum coefficient of performance of a real device by using the conventional ZT formulas. Thus $Z\bar{T}_{\text{eff}}$ is a useful concept for the design engineer because it is a measure of the TE material quality over a large ΔT.

III. EXPERIMENTAL SYSTEM

Conceptually the experimental system is similar to that shown in Fig. 1 but a few complications exist. One requirement for testing a TE sample is that the sample must be a device-ready leg with metallization on both ends. For Bi_2Te_3-based TE elements, the metallization material most commonly used is Ni, and its purpose is to allow soldering with low electrical and thermal contact resistances while acting as a diffusion barrier.[13] In the following analysis, no distinction is made between the intrinsic properties of the bulk and the properties of the contact. If significant contact resistances are present, they will be automatically lumped into the effective properties. Most samples that were measured had electrical contact resistances estimated to be $<5\%$ of the total resistance. The sample was a Bi_2Te_3 p-type leg from Marlow Industries with dimensions of approximately $1.6\times1.6\times1.6$ mm^3.

Figure 2(a) illustrates the system designed to measure the device properties and energy conversion efficiency of the TE leg. The system is composed of the following elements: the hot assembly, the TE leg, the cold assembly, and the surrounding vacuum chamber. The hot assembly is soldered to the top of the leg and consists of a calibrated electrical heater providing Q_H, a thermocouple measuring T_H, and an electrode conducting I. The cold assembly is soldered to the cold side of the leg and consists of a copper heat spreader, a thermocouple measuring T_C, an electrode, a calibrated thermopile type heat flux sensor measuring Q_C, and a heater used for calibration. The bottom side of the heat flux sensor is mounted to a TE cooler module which was used in the efficiency measurement to control T_C independent of T_∞ in order to reduce heat losses at the cold assembly. The electrodes supply current to the TE leg for the resistance and efficiency measurements and are controlled by an external power supply. The entire assembly is contained in a vacuum chamber at a pressure of 5×10^{-5} Torr and a uniform ambient temperature, T_∞ of 22–24 °C.

Prior to mounting the leg, the hot assembly was suspended [Fig. 2(b)] and calibrated for heat loss. In this case the Joule heating IV_{Heater} will be balanced by the radiation and conduction losses. The hot assembly electrode is very thin to minimize heat conduction losses but this means it

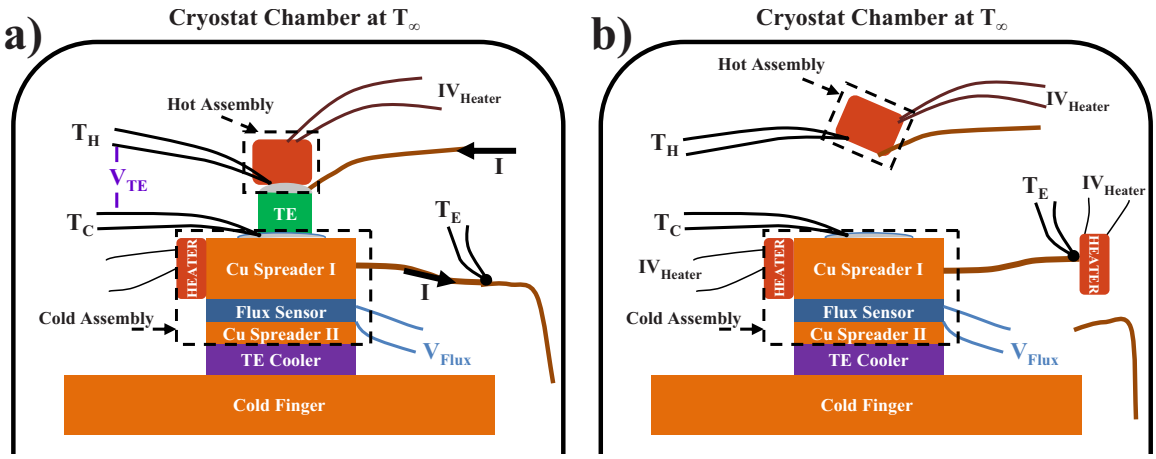

FIG. 2. (Color online) A schematic diagram of the (a) property and efficiency measurement system and (b) calibration procedure for the hot side heater and the cold side heat flux sensor.

produces a relatively large unknown Joule heating term for $I \neq 0$ and thus Q_H cannot be accurately measured during the efficiency measurement. Radiation losses at the cold assembly are negligibly small. The primary heat loss is from conduction along the electrode, which is much thicker than the hot assembly electrode. In order to calibrate the flux sensor the cold assembly electrode was disconnected from the outside circuit. The voltage response of the flux sensor was measured for different heat fluxes imposed by the calibration heater, which is mounted to the side of the cold assembly. After the flux sensor calibration, the thermal conductance of the electrode was measured by mounting another heater to the end of the electrode and measuring the temperatures T_E and T_C [Fig. 2(b)], in which the radiation loss of the electrode is negligible compared with the heat conduction along the electrode. The electrical resistance between the positions of T_E and T_C was measured, which allows us to solve for the Joule heating inside the electrode when $I \neq 0$. We correct for Joule heating in Q_C but not in Q_H, therefore we rely only on Q_C during the efficiency measurement.

In our calibration it was found that heat losses from the hot assembly constituted about 10% of Q_H. At the cold assembly heat conduction loss was dominant to Joule heating in the electrode, and the combined correction value constituted $<3\%$ of Q_C. We performed an energy balance over the leg such that $Q_{\text{rad,side}} = Q_{H,OC} - Q_{C,OC}$ with $\Delta T = 75\ ^\circ\text{C}$ and solved for the emissivity. The obtained emissivity of $\varepsilon = 0.6$ agrees reasonably with Fourier transform infrared spectroscopy measurements from similar samples and in addition is evidence that the heater and flux sensor have been accurately calibrated.

IV. PROPERTY DATA ANALYSIS

The procedure for the properties measurement is to set a constant heater power, wait for the system to reach steady state, and then measure V_S, $Q_{H,OC}$, and R from Sec. II B. Then the heater power is reset and the properties are measured again for different values of T_H and T_C. Although it is possible to control the cooler module for each successive heater power setting to keep T_C constant, this increases steady state settling times considerably and adds unnecessary complexity. Due to temperature drifts in the system, $Q_{C,OC}$ had larger uncertainties than $Q_{H,OC}$ for small temperature differences where $Q_{C,OC} < 0.1$ W. Therefore, during the properties measurement, in order to capture the entire temperature range from ΔT of 2 °C to 160 °C, we use $Q_{H,OC}$ instead of $Q_{C,OC}$ and allow T_C to rise with increasing T_H (Fig. 3).

Based on the integral relationship between the intrinsic properties and the device properties, the intrinsic properties can be solved for by regression fitting or taking the numerical derivative of the device properties. We found that the latter method was more accurate. The process can be understood by considering an arbitrarily measured device property $Y(T_H, T_C)$ and an intrinsic property $y(T)$ related by

$$Y(T_H, T_C) = \int_{T_C}^{T_H} y(T)dT = f(T_H) - f(T_C), \tag{15}$$

where $\partial f(T)/\partial T = y(T)$. We take the derivative with respect to T_H,

$$\frac{dY(T_H, T_C)}{dT_H} = \frac{df(T_H)}{dT_H} - \left.\frac{\partial f(T_C)}{\partial T_C}\right|_{T_H} \frac{dT_C}{dT_H} = y(T_H) - y(T_C)\frac{dT_C}{dT_H}, \tag{16}$$

and evaluate the derivatives numerically. Taking the centered

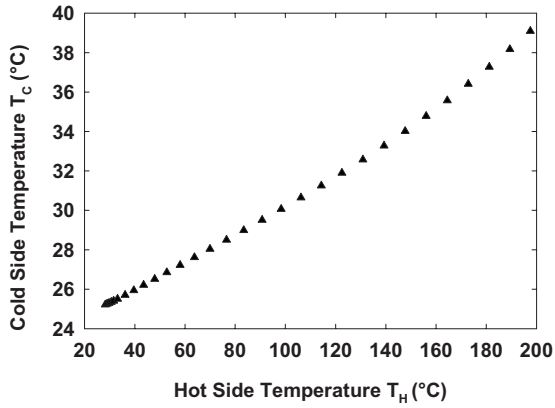

FIG. 3. Cold side temperature vs hot side temperature during the device properties measurement.

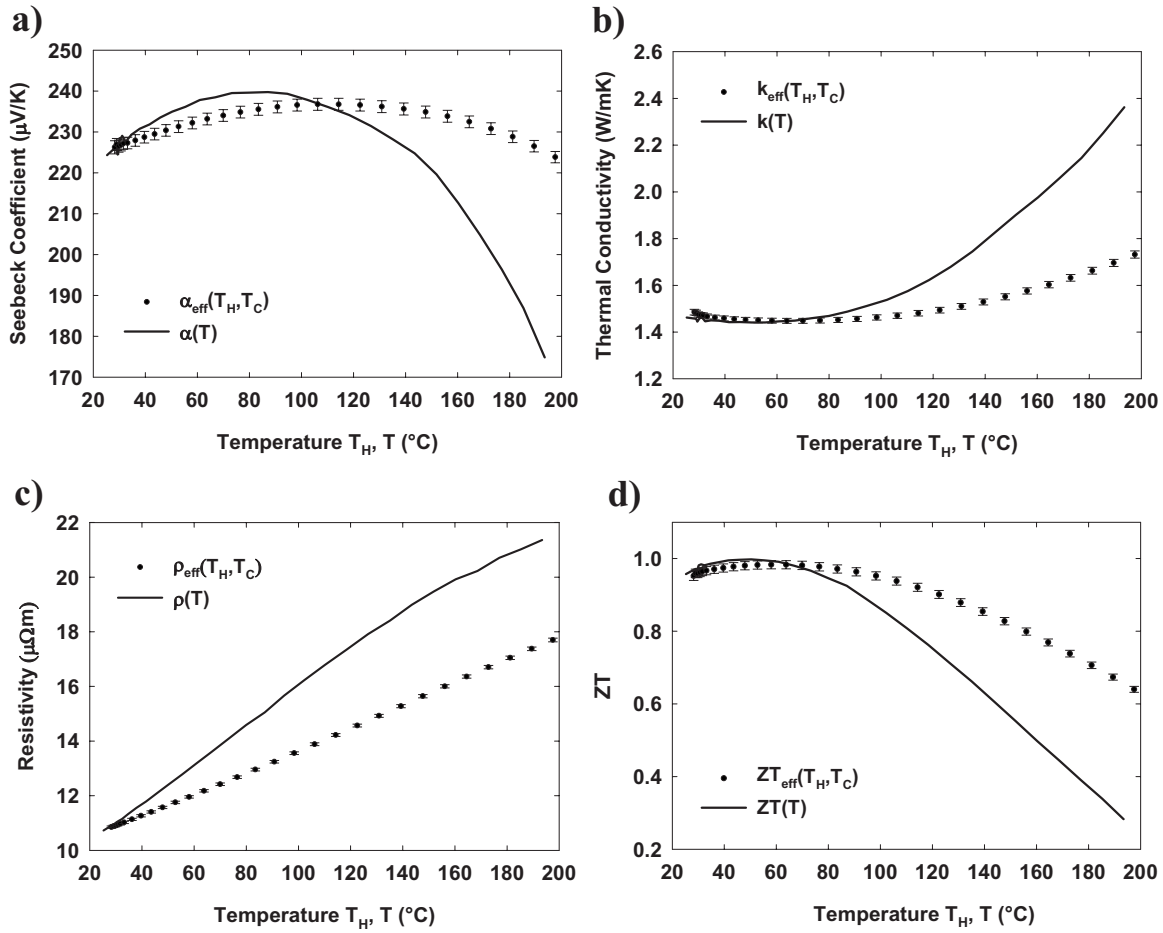

FIG. 4. The four TE properties vs temperature and their respective effective properties vs hot side temperature: (a) Seebeck coefficient, (b) thermal conductivity, (c) electrical resistivity, and (d) dimensionless TE figure of merit.

difference, we solve for the arbitrary property as a function of temperature

$$y(\bar{T}_H) = \frac{\Delta Y}{\Delta T_H} + y(\bar{T}_C)\frac{\Delta T_C}{\Delta T_H}, \tag{17}$$

where $\bar{T}_H = (T_{H,2} + T_{H,1})/2$ is the mean temperature of two consecutive measurements. We observe from Fig. 3 that $\Delta T_C/\Delta T_H \approx 0.08$ so it is important to evaluate the properties accurately in the low temperature range because they will also affect the higher temperature range. A linear regression fit was applied to the first few measurement points in the lower temperature range.

V. PROPERTY RESULTS

Each of the intrinsic properties from Sec. II was evaluated by taking the numerical derivative of the device properties following the procedures described in Sec. IV. Figures 4(a)–4(d) plot $\alpha(T)$, $\rho(T)$, $k(T)$, and $Z\bar{T}(T)$ as well as their respective effective properties as a function of T_H. The measured effective properties are plotted as discrete points with error bars while the intrinsic properties have been plotted as linearly interpolated curves. The uncertainty was estimated individually for each effective property point. The maximum uncertainty values for α_{eff}, k_{eff}, and ρ_{eff} are approximately 0.7%, 0.9%, and 0.4%, respectively. Figure 4(d) shows that $Z\bar{T}$ drops off with increasing temperature more rapidly than $Z\bar{T}_{\text{eff}}$ due to the integral relationship between the intrinsic and effective properties. This graph can be used by the design engineer to quickly determine the performance of a TE generator made with this leg. For instance, given $T_H = 198$ °C and $T_C = 39$ °C (Fig. 3), the leg should operate as a $Z\bar{T} = 0.64$ material. To verify that the intrinsic property curves have been differentiated correctly we used the intrinsic prop-

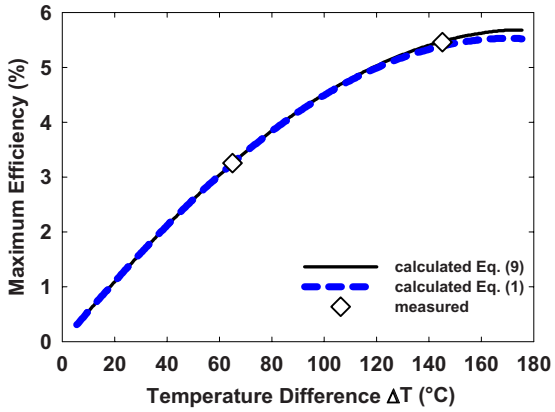

FIG. 5. (Color online) Maximum efficiency vs temperature difference across the leg for a cold side temperature of 24.5 °C.

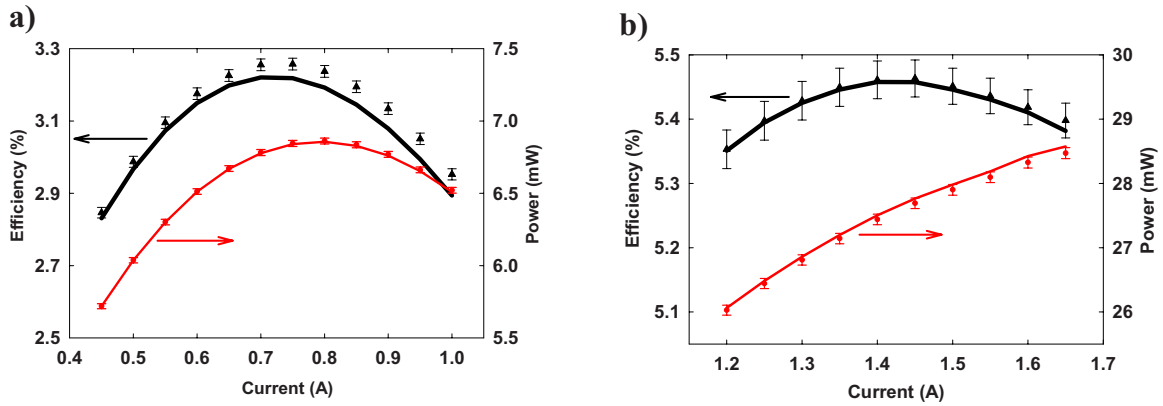

FIG. 6. (Color online) Efficiency and power vs current, the points with error bars are the measured values, the lines are calculated from the measured properties using Eqs. (9) and (10). (a) Hot side temperature is 86–93 °C, cold side is 24–25 °C. (b) Hot side temperature is 169–172 °C.

erties to solve for $Z\bar{T}_{\text{eff}}$ at the same measured temperature points as in Fig. 4(d) and found the relative difference to be 0.2%.

VI. EFFICIENCY RESULTS

The goal of the efficiency measurement is to firmly establish what performance can be expected from the particular leg and to compare these results to the calculated power and efficiency from the intrinsic properties measurement. The procedure was to apply a constant heater power and current, measure the steady state Q_C, P_e, and then repeat for another current setting. The efficiency was measured at two different temperature ranges, the estimated uncertainty was less than 0.6%.

Figure 5 plots the maximum efficiency versus ΔT for T_C=24.5 °C. The solid curve is the calculated value from the intrinsic property data using Eq. (9), the dotted curve is using Eq. (1) with the calculated $Z\bar{T}_{\text{eff}}$ from Eq. (14) and the discrete points are measured values. Equations (1) and (9) show excellent agreement for $\Delta T < 120$ °C, which confirms that it is appropriate to characterize a material by $Z\bar{T}_{\text{eff}}$. The small divergence at high ΔT reflects that $\alpha(T)$ drops rapidly at high temperature and the assumption $\alpha(T_H) \approx \alpha(T_C) = \alpha_{\text{eff}}$, [Eq. (14)], is not well satisfied.

Figures 6(a) and 6(b) plot the measured and calculated efficiency [Eq. (9)] versus current at both temperature ranges. The calculated and measured powers are in excellent agreement for both cases with a relative difference of <0.4% for all measured points. The relative difference of measured to calculated efficiency in Fig. 6(a) is 0.5%–2.0% while that for Fig. 6(b) is 0.1%–0.3%. The larger relative difference of efficiency in Fig. 6(a) is likely an indication of the larger uncertainty in Q_C at small heat transfers rates.

Recall that $Q_{H,OC}$ and Q_C are independently measured quantities with independent calibrations. The property measurement uses $Q_{H,OC}$ and the efficiency measurement uses Q_C. Therefore, the fact that the measured power and efficiency are in excellent agreement with each other is convincing evidence that both have been measured accurately. This independent check feature is an important advantage of the described technique.

VII. CONCLUSION

In this work, we employ an effective property approach to model a single TE leg for power generation. We apply a one-dimensional model considering temperature-dependent material properties and side wall radiation loss. Using effective properties, we are able to write approximate solutions for the power and efficiency, which are mathematically similar to the well-known constant property formulas. If the Seebeck coefficient varies strongly over the operating temperatures, the Thompson heat should be included in the efficiency calculation for most accurate results.

We developed an experimental technique capable of directly measuring an energy balance over a single leg, with a large temperature difference ranging from 2 °C to 160 °C. The technique measures all three TE properties of a single leg, in the same direction, with significantly less uncertainty than other methods. The measurements include the effects of temperature dependent properties, side wall radiation, and contact resistance. Side wall radiation loss constituted <2% of the hot side heat transfer rate, but it is still a significant part of the energy balance considering that the power conversion efficiency was 2.8%–5.5%. The power and efficiency were directly measured and are within 0.4% and 2% of the values calculated based on the property measurements.

ACKNOWLEDGMENTS

The authors acknowledge financial support from MASDAR for the efficiency measurement, DOE (Grant No. DE-FG02-08ER46516) for the property measurement, and KFUPM for modeling.

APPENDIX

Integrating Eq. (4) once with respect to x gives

$$kA\frac{dT}{dx} + \frac{I^2}{A}\int_0^x \rho dx' - I\int_{T_H}^{T} \tau dT' - \varepsilon\sigma_{\text{sb}}P\int_0^x (T^4 - T_\infty^4)dx' + C_1 = 0, \quad \text{(A1)}$$

where $\tau = Td\alpha/dT$ is the Thompson coefficient and C_1 is a constant of integration. We integrate a second time with respect to x and apply the boundary conditions $T|_{x=0} = T_H$ and

$T|_{x=L}=T_C$ to solve for the integration constants

$$-kA\frac{dT}{dx}=\frac{I^2}{A}\int_0^x \rho dx' - I\int_{T_H}^{T}\tau dT' - \varepsilon\sigma_{sb}P\int_0^x (T^4 - T_\infty^4)dx' - \frac{A}{L}\int_{T_H}^{T_C} kdT + \frac{\varepsilon\sigma_{sb}P}{L}\int_0^L\int_0^x (T^4 - T_\infty^4)dx'dx - \frac{I^2}{LA}\int_0^L\int_0^x \rho dx'dx + \frac{I}{L}\int_{T_H}^{T_C}\int_{T_H}^{T}\tau dT'dT. \quad \text{(A2)}$$

After rearranging terms we solve for the temperature gradient at the hot side

$$-kA\frac{dT}{dx}\bigg|_{T_H}=\frac{A}{L}\int_{T_C}^{T_H} kdT + \frac{\varepsilon\sigma_{sb}P}{L}\int_0^L\int_0^x (T^4 - T_\infty^4)dx'dx - I^2R\left(\frac{\int_0^L\int_0^x \rho dx'dx}{L\int_0^L \rho dx}\right) - I\beta\left(\frac{\int_{T_H}^{T_C}\int_{T_H}^{T'}\tau dT'dT}{L\int_{T_H}^{T_C}\tau dT}\right), \quad \text{(A3)}$$

where $\tau=Td\alpha/dT$ is the Thompson coefficient. If we assume that the quantities in the parenthesis are approximately equal to $\frac{1}{2}$, then we can apply this result to Eq. (2) to derive Eq. (12).

Applying $I=0$ results in Eq. (6), which is composed of a heat conduction term and a radiation term given by

$$Q_{rad}=\frac{\varepsilon\sigma_{sb}P}{L}\int_{T_C}^{T_H}\int_{T}^{T_H}\frac{(T'^4 - T_\infty^4)}{\frac{dT'}{dx}\frac{dT}{dx}}dT'dT \approx \frac{\varepsilon\sigma_{sb}PL}{\Delta T^2}\int_{T_C}^{T_H}\int_{T}^{T_H}(T'^4 - T_\infty^4)dT'dT. \quad \text{(A4)}$$

This is the additional hot side heat transfer at $x=0$ due to side wall radiation. We integrate the radiation along the length of the leg to solve for the total side wall radiation loss

$$Q_{rad,side}=\varepsilon\sigma_{sb}P\int_{T_H}^{T_C}\frac{(T^4 - T_\infty^4)}{\frac{dT}{dx}}dT \approx \frac{\varepsilon\sigma_{sb}PL}{\Delta T}\int_{T_C}^{T_H}(T^4 - T_\infty^4)dT. \quad \text{(A5)}$$

Both radiation quantities have been approximated by assuming a linear temperature gradient.

[1] T. Hendricks, "Engineering Scoping Study of Thermoelectric Generator Systems for Industrial Waste Heat Recovery," U.S. Department of Energy, 2006.
[2] T. C. Harman, J. H. Cahn, and M. J. Logan, J. Appl. Phys. **30**, 1351 (1959).
[3] H. J. Goldsmid, *Electronic Refrigeration* (Pion, London, 1986).
[4] H. Iwasaki, M. Koyano, and H. Hori, Jpn. J. Appl. Phys., Part 1 **41**, 6606 (2002).
[5] A. Satake, H. Tanaka, T. Ohkawa, T. Fujii, and I. Terasaki, J. Appl. Phys. **96**, 931 (2004).
[6] R. Venkatasubramanian, E. Siivola, T. Colpitts, and B. O'Quinn, Nature (London) **413**, 597 (2001).
[7] H. Iwasaki and H. Hori, *Proceedings of the 24th International Conference on Thermoelectrics (ICT 2005)* (IEEE, New York, 2005), pp. 513–516.
[8] L. J. v. d. Pauw, Philips Res. Rep. **13**, 1 (1958).
[9] J. A. Cape and G. W. Lehman, J. Appl. Phys. **34**, 1909 (1963).
[10] M. Gao and D. M. Rowe, Meas. Sci. Technol. **8**, 1261 (2001).
[11] D. M. Rowe, *Thermoelectrics. CRC Handbook* (CRC, Boca Raton, FL, 1995).
[12] B. Sherman, R. R. Heikes, and R. W. Ure, Jr., J. Appl. Phys. **31**, 1 (1960).
[13] T. Caillat, J. P. Fleurial, G. N. Snyder, A. Zoltan, D. Zoltan, and A. Borshchevsky, *Proceedings of the 18th International Conference on Thermoelectrics*, (IEEE, New York, 1999), pp. 473–476.
[14] T. Caillat, J. P. Fleurial, G. J. Snyder, and A. Borshchevsky, *Proceedings of the 20th International Conference on Thermoelectrics (ICT 2001)*, (IEEE, New York, 2001), pp. 282–285.
[15] N. W. Ashroft and N. D. Mermin, *Solid State Physics* (Brooks/Cole Thomson Learning, 1976).
[16] R. W. Diller and L. E. Bell, *Proceedings of the 22nd International Conference on Thermoelectrics (ICT 2003)*, (IEEE. New York, 2003), pp. 571–573.
[17] P. M. Mayer, *Department of Electrical Engineering and Computer Science* (MIT, Cambridge, 2007), p. 269.
[18] M. Gao, D. M. Rowe, and K. Kontostavlakis, J. Phys. D: Appl. Phys. **8**, 1301 (2004).